Materials Science and Engineering A 527 (2010) 3057–3063

Contents lists available at ScienceDirect

Materials Science and Engineering A

journal homepage: www.elsevier.com/locate/msea

Study on fatigue property of a new 2.8 GPa grade maraging steel

Wei Wang[a,c], Wei Yan[a], Qiqiang Duan[b], Yiyin Shan[a], Zhefeng Zhang[b], Ke Yang[a,*]

[a] Institute of Metal Research, Chinese Academy of Sciences, Shenyang 110016, China
[b] Shenyang National Laboratory for Materials Science, Institute of Metal Research, Chinese Academy of Sciences, Shenyang 110016, China
[c] Graduate University of Chinese Academy of Sciences, Beijing 10049, China

ARTICLE INFO

Article history:
Received 31 August 2009
Received in revised form 9 December 2009
Accepted 1 February 2010

Keywords:
Maraging steel
Fatigue property
S–N curve
Fatigue crack

ABSTRACT

A new 2.8 GPa grade maraging steel was developed in the present work and the tension–tension fatigue property of the steel was studied after peak-aging treatment. The results showed that the steel could reach an ultimate tensile strength of 2760 MPa, a fracture toughness of 31.6 MPa $m^{1/2}$, and a fatigue limit of 1150 MPa at stress ratio of 0.1. It was revealed that the fatigue crack initiation of the steel mainly originated from the surface at high stress level but from the interior inclusions at low stress level. From the observations by transmission electron microscope (TEM) and fatigue crack propagation curves, it was proposed that the cyclic softening occurred, which was induced by the resolution as well as the growth of precipitates, and the poor fatigue crack growth resistance and high fatigue crack propagation rate might be the main reason for the relatively low fatigue limit of the steel.

1. Introduction

Maraging steels exhibit unique combinations of ultra-high strength and excellent fracture toughness, and are taken as important material candidates for critical applications such as rocket engine cases, submarine hulls and cryogenic missiles [1–4]. The automobile manufacturers and corresponding component suppliers of all over the world have been looking for ultra-high-strength materials for weight reduction or other reasons, in which maraging steel with super-high strength can be considered as a new choice. Except for the high tensile strength, the fatigue property becomes another critical issue to be focused because most of the components often serve under cyclic loading condition. However, regarding to the ultra-high strength of maraging steels, their fatigue strength is found to be far below the expected value which is usually empirically predicted by taking half of the ultimate tensile strength of steels. In order to improve the fatigue strength of the maraging steels and hence extend their applications, an effective way is to reduce the content of those elements harmful to the fatigue property and the relevant fatigue fracture mechanism needs to be deeply investigated [5–7].

In the present work, based on progresses of the previous studies [3,6–8], a new maraging steel with high Ni, Ti and low Mo contents, possessing an ultimate tensile strength up to 2.8 GPa and fracture toughness above 30 MPa $m^{1/2}$, was developed to study its fatigue behavior after the peak-aging treatment. Additionally, the fatigue fracture mechanism of this maraging steel was also discussed.

2. Experimental procedure

The experimental steel was melted in a 300 kg vacuum induction melting furnace at first, and then was remelted in a vacuum arc melting furnace. After homogenization at 1250 °C for 24 h, the ingot was rolled to a cross-section dimension of 55 mm × 55 mm, which was finally forged into rods with 22 mm in diameter followed by air-cooling. The final chemical composition of the steel is listed in Table 1.

The specimens for tests were cut from the middle part of the forged rods, and those for tensile and fatigue tests were cut with the load direction in accord with the rolling direction. Specimens were solution treated at 820 °C for 1 h followed by a cryogenic treatment in liquid nitrogen for 1 h to remove the retained austenite, and then were aged at different temperatures and times. Tensile test was carried out with an MTS810 testing machine at a crosshead speed of 2 mm/min, and each result was taken from an average of three tests. For the fatigue test, the frequency was 104 Hz with a sine wave, and the stress ratio was 0.1. The dimension of fatigue specimen is shown in Fig. 1a. The plane strain fracture toughness (K_{IC}) was measured using three-point bending method in accordance with ASTM E399 specification and the value of K_{IC} was taken from an average of three tests. The dimension of specimen for K_{IC} measurement is shown in Fig. 1b. All the tests were conducted at room temperature in air.

Specimens after aging treatment were mechanically ground and polished for microhardness test with load of 500 g and loading

* Corresponding author. Tel.: +86 24 23971628; fax: +86 24 23971517.
E-mail address: kyang@imr.ac.cn (K. Yang).

0921-5093/$ – see front matter © 2010 Elsevier B.V. All rights reserved.
doi:10.1016/j.msea.2010.02.002

Table 1
Chemical compositions of the experimental maraging steels (wt%).

Ni	Co	Mo	Ti	C	S	P	O	N
17.7	14.7	6.73	1.23	0.003	0.003	0.004	0.002	0.0015

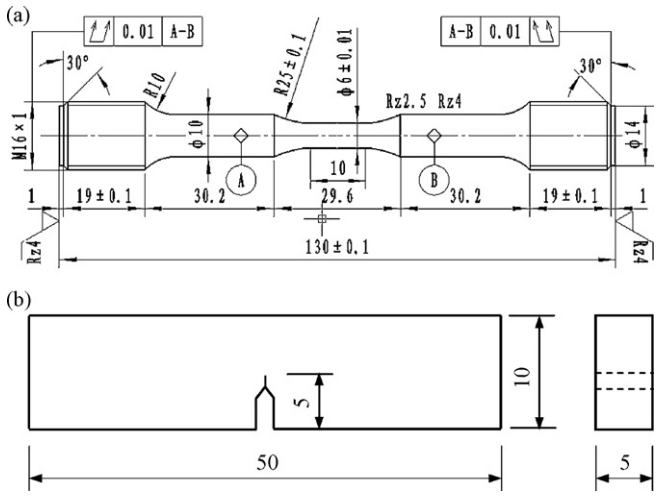

Fig. 1. Dimension of specimen for fatigue test and K_{IC} measurement. (a) Dimension of specimen for fatigue test; (b) dimension of specimen for K_{IC} measurement.

time of 15 s. The microstructure of the specimens after peak-aging treatment was examined under optical microscopy after etched by 10% nital solution. The fracture morphologies were observed after fatigue test on a scanning electron microscopy (SEM). Transmission electron microscopy (TEM) was used to examine the distribution of precipitations in the steel.

3. Results and discussions

Variation of hardness of the experimental steel as a function of aging time at different aging temperature is shown in Fig. 2. It can be found that the aging responses were fairly rapid at 480, 500 and 520 °C, and nearly 90% of the total hardness increase could be attained within the first 45 min of aging. A maximum hardness of HRC62.1 was obtained at 500 °C within about 2 h and then a slight over-aging occurred with increase of time. However, at temperature of 520 °C, the hardness began to decline at about 2 h, which is relatively earlier for the steel. It is well known that at higher aging temperature, with increase of time, Ni is inclined to aggregate along the martensite grain boundary as well as local region in the martensite lath such as the place with high density dislocations and stack faults, and the region with clustering of Ni contributes to the reconstruction of lattice, which can lead to the formation

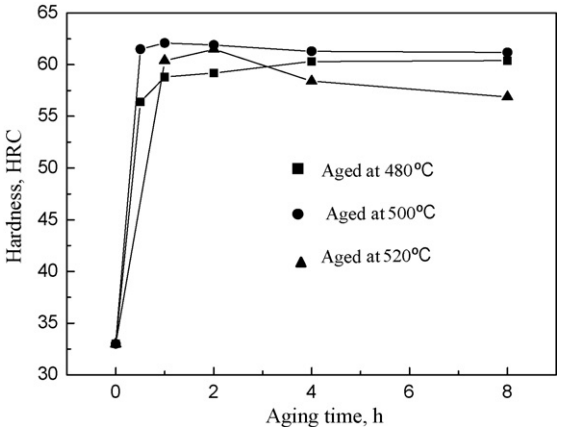

Fig. 2. Effects of aging temperature and time on the hardness of the maraging steel.

Table 2
Mechanical properties of peak-aged maraging steel.

σ_b (MPa)	$\sigma_{0.2}$ (MPa)	Δ (%)	Ψ (%)	K_{IC} (MPa m$^{1/2}$)
2760	2650	7.0	31.2	31.6

of reversed austenite. The formation of reversed austenite could make the decrease of the hardness of the steel. Based on the above results, the optimum heat treatment procedure (peak aging) could be determined as the following: 820 °C/1 h + cryogenic treatment in liquid nitrogen/1 h + 500 °C/2 h.

Fig. 3 shows the optical micrographs of the experimental steel after peak aging at 500 °C for 2 h. The prior austenite grain size was measured to be about 30 μm, and the steel had got full of low-carbon martensite structure without retained austenite, as shown in Fig. 3. Fig. 4 represents the TEM images of the peak-aged steel. It can be seen from the bright field image (Fig. 4a) that the microstructure of the steel consisted of lath martensite with high density of dislocations. The dark field image (Fig. 4b) shows that great deals of needle-like precipitates in nanometer size well homogenously distributed in the matrix. It can be identified from the SAD pattern (as shown in Fig. 4c) that the precipitate should be a Ni_3 (Mo, Ti) type phase. The un-dissolved coarse precipitates reported in other studies [9–11] such as μ-$(Fe, Co)_7Mo_6$, σ-Fe_2Mo, Ni_4Mo, were not found in the matrix.

Table 2 lists the results of the tensile and plane strain fracture toughness (K_{IC}) tests on the maraging steel after peak-aging treatment. It can be seen that the ultimate tensile strength (UTS) could reach over 2700 MPa due to the removal of the retained austenite at cryogenic temperature and the higher alloying in the steel. On the other hand, the fracture toughness did not fall down sharply and still remained a relatively high level. The relationship between the

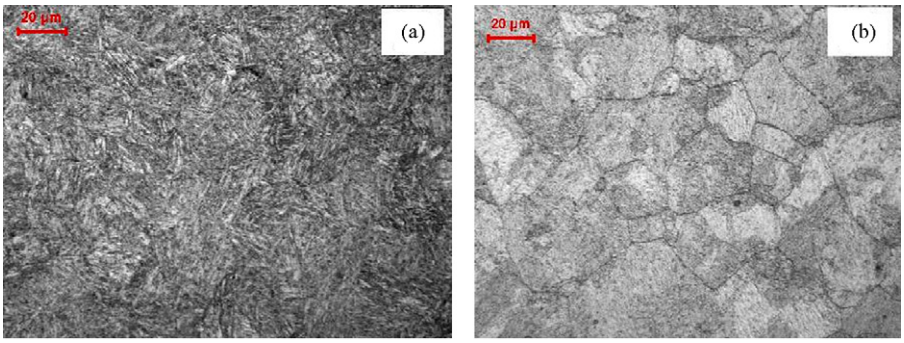

Fig. 3. Optical micrographs of the maraging steel: (a) low-carbon matensites; (b) prior austenite grains.

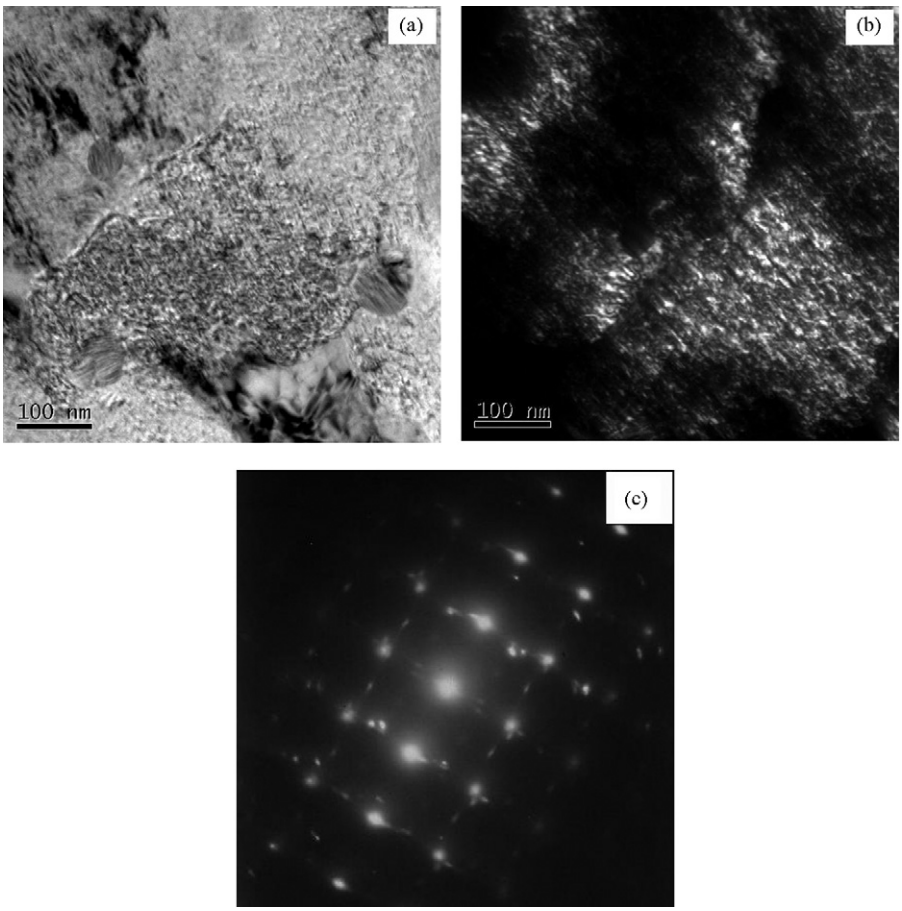

Fig. 4. TEM images of the maraging steel after peak-aging: (a) bright field image, showing the martensite lath morphology; (b) dark field image, showing the distribution of Ni_3 (Mo, Ti) type phase; (c) PAD pattern of the matrix and precipitates.

UTS and optimum fracture toughness of some other grades maraging steels are shown in Fig. 5 [5–8,12–14]. It is clearly shown that the UTS of a 13Ni (4 0 0) maraging steel was only 2570 MPa, which is much lower than the designed value. Although the strengths of other steels got certain improvements by the special complicated thermo-mechanical and cold-rolling treatments, their fracture toughness is still lower than that of the steel in the present work.

The S–N curve obtained in this work is shown in Fig. 6. It can be seen that the S–N curve approximately consists of three linear relations, one corresponds to the low-cycle fatigue life at higher stress level and another is the ultra-long fatigue life at lower stress level. The transition from short to ultra-long fatigue life appears usually as a horizontal step in an S–N curve. The fatigue limit σ is determined as the highest stress at which the specimen has run out to the cyclic number of 10^7 without failure. The horizontal portion of the S–N curves in Fig. 6 indicates that the fatigue limit of the maraging steel is approximately 1150 MPa.

The fatigue fracture photographs of the failed specimens are shown in Figs. 7 and 8. Fig. 7 shows the fatigue fractograph of the maraging steel at a high cyclic stress of 1500 MPa. It can be clearly found from Fig. 7(a) that the fatigue crack firstly initiated at the specimen surface and no inclusion was found in the initiation site. In addition, the entire fracture surface can be separated into three

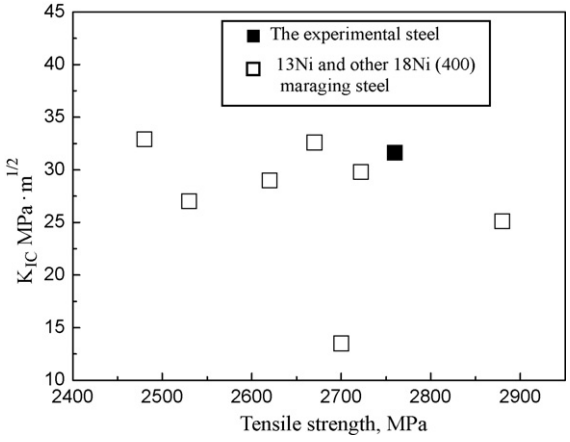

Fig. 5. Tensile strength versus K_{IC} of 13Ni and 18Ni maraging steels.

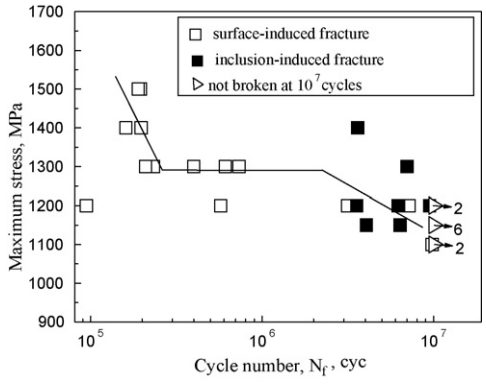

Fig. 6. S–N curve of the maraging steel, frequency: 104 Hz, stress ratio: 0.1, frequency shape: sine curve.

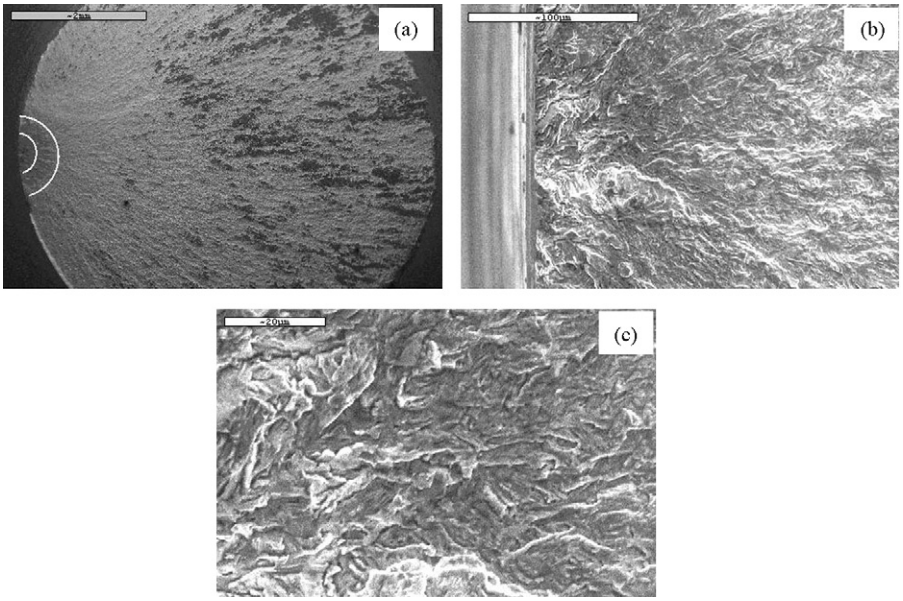

Fig. 7. Fractograph of the surface-induced fracture ($R = 0.1$, $\sigma_{max} = 1500$ MPa, $N = 5.53 \times 10^4$ cycles). (a) Macro-image of fracture surface; (b) macro-image of surface crack origin; (c) high-magnification photograph near the surface crack origin.

typical areas as indicated by a couple of lines and arrows in Fig. 7(a). The first area is a flat area inside the first semi-ellipse line. The second is a sandwiched area between couple of the semi-ellipse lines, which has the characteristic morphology with distinct roughness. The third is a wide fracture surface having many radial streaks in accordance with the crack propagation direction. Thus, the fracture surface from the surface-induced fracture along the axial loading can be divided into the following three areas: (i) a flat area at the initial stage, (ii) a rough area outside the initial flat area, and (iii) a wide fracture surface having the radial ridge pattern outside the rough area. The fatigue fracture mode under the above condition was a transgranular quasi-cleavage failure, in which there were a few secondary cracks and rub marks, but the fatigue striation could not be found on the whole fracture surface (as shown in Fig. 7(b) and (c)).

Fig. 8 gives another example of the fracture surface at a low cyclic stress of 1200 MPa. Fig. 8(a) presents an overall fracture surface under a low magnification and Fig. 8(b) is a magnified observation around a fish-eye. In these two photographs, the fracture surface can be clearly separated into three characteristic areas as described above. Fig. 8(c) and (d) shows the corresponding high-magnification photograph around the inclusion at the crack initiation site and the EDS analysis result on an interior inclusion. It was identified that the interior inclusion was Al_2O_3, with diameter of about 13 μm. In this work, even by a highly purified melting, non-metallic inclusions such as Al_2O_3 could not be fully excluded

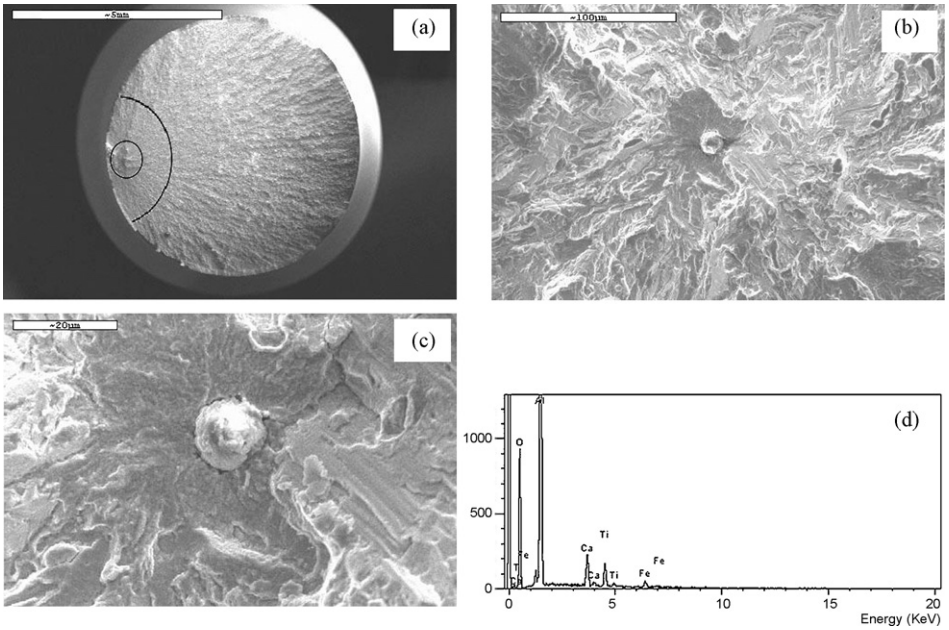

Fig. 8. Fractograph of the interior inclusion-induced fracture with a fish-eye ($R = 0.1$, $\sigma_{max} = 1200$ MPa, $N = 9.50 \times 10^6$ cycles): (a) macro-image of fracture surface; (b) fractograph around a fish-eye; (c) high-magnification photograph at fish-eye; (d) the EDS analysis on the interior inclusion.

in the steel, as shown in Fig. 8. It is quite common for the heat-treated steels, especially those ultra-high strength steels, to have some residual stress and even accumulate some hydrogen atoms around those non-metallic inclusions. It is also well known that the coefficient of thermal expansion of Al_2O_3 is smaller than that of the steel matrix, and the residual stress at the equator of such a globular inclusion is supposed to be tensile [15–17]. Based on the recent work [18,19], it has been directly verified by using secondary ion mass spectrometry that the interface of inclusions could trap hydrogen atoms. They assumed that, as a result of superposition of the applied cyclic loading, residual stress and existence of hydrogen, the initiation and growth of cracks from internal non-metallic inclusions take place due to the hydrogen-assisted cracking. After a slow fatigue crack growth in the area beside the inclusion, the size of the crack can exceed a critical size given by the threshold for pure fatigue propagation, and the crack will grow without the assistance of hydrogen by producing a fatigue surface in the typical martensite lath microstructure. Therefore, it can be assumed that the fatigue cracking of the present steel is an interior inclusion-induced fracture at lower stress level.

In addition, the fatigue fracture surfaces of all the specimens were observed by SEM. It is found that the fatigue crack initiation sites mainly originated either from the specimen surface or from the interior inclusions. It can be seen from Fig. 6, at high cyclic stress level up about 1300 MPa, most the fatigue cracks initiated form the specimen surfaces; however, the fatigue cracks inclined to originate from the interior inclusions at low cyclic stress level of below 1300 MPa. This indicates that there is a clear transition of fatigue cracking initiation from surface to the interior at the critical cyclic stress level of about 1300 MPa. This critical cyclic stress level should be associated with the microstructure, size of inclusions, tensile strength as well as the loading mode or stress ratio.

Some researchers have reported the fatigue properties of maraging steels with different tensile strength levels [7,20–22]. These results showed that the increase of tensile strength could not lead to an improvement of the fatigue properties, even after shot peening or nitriding to the steels, and the fatigue strength was far below the expected value which was predicted empirically to be a half of the ultimate tensile strength. Although the fatigue strength of the present steel was about 1150 MPa, lower but close to the half of the tensile strength, it should be noted that the experiment was conducted by the axial loading and the stress ratio was 0.1. If the Goodman relationship is used to equivalently transform the fatigue limit tested with stress ratio of 0.1 to that with stress ratio of −1, the fatigue limit is found to be only 693 MPa, less than 30% of the tensile strength, as reported by others [23]. The poor fatigue property of maraging steels compared with their ultra-high tensile strength may be partly attributed to the detrimental effect of the water vapor in the ambient air or the rough surface conditions. However the reason for attributing the low fatigue strength of maraging steels not only to the structural instability but also to the poor fatigue crack growth resistance may be clear from the following observations and analyses.

First, comparison of the precipitates in the steel before and after cyclic deformation revealed that the later showed an increase in size of the precipitates, especially after 10^7 cycles, as shown in Fig. 9. The size of the precipitates before cycling was 5–10 nm, but exceeded 10 nm after 10^7 cycles, and the SAD showed that the

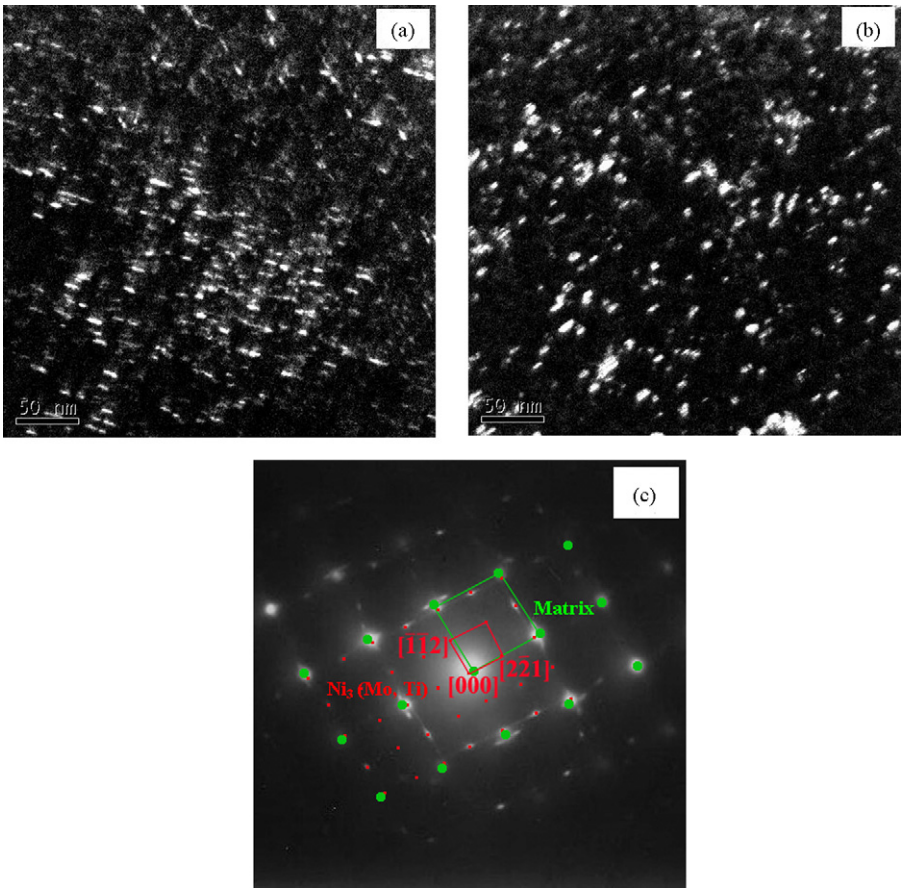

Fig. 9. TEM images and corresponding diffraction pattern of precipitates in the maraging steel before and after cyclic deformation: (a) dark field image, before cyclic deformation, size of precipitates was 5–10 nm; (b) dark field image, after 10^7 cycles deformation, precipitates were coarsened exceeding 10 nm; (c) PAD pattern of the precipitates.

precipitates were Ni_3Mo intermetallic compounds which are the main hardening precipitates in maraging steels. It was reported that during the process of cyclic hardening and softening in precipitation-hardened alloys the geometry and distribution of precipitates as well as the dislocation–particle interaction could be altered by cyclic straining [5,7]. As one of typical precipitation-hardened alloys, maraging steels contain fine and closely spaced precipitates which are coherent with the matrix and can be easily sheared by dislocations. It is generally believed that cyclic softening is highly favored by this particularly interesting feature of these alloys. Therefore it can be considered that during the cyclic softening of the present steel, cyclic straining could produce the resolution of some precipitates and the growth of some other precipitates, the aggregation of Ni-rich precipitates would induce the formation of soft regions in which further deformation would be localized and the probability of crack nucleation could be significantly increased. The electron diffraction patterns of the peak-aged steel before and after cyclic deformation also showed that the diffraction spots of precipitates became scattering as a result of cycling. This phenomenon should be attributed to the high elastic stresses around the precipitates, which might cause the diffraction to bend and rotate with respect to the matrix.

Van Swam et al. [7] studied the fatigue behavior of a 300 series maraging steel and found that the lower fatigue limit of the steel could be attributed to the extensive cyclic softening during fatigue process, with a mechanism of dislocation rearrangement and dislocation–precipitate interaction. Neither resolution nor growth of precipitates was clearly identified in their study. It should be noted that after 10^7 cycles, the ultimate tensile strength of the present steel was found to decrease to 2543 MPa, 6% reduction compared with that before the cyclic deformation, which further demonstrates the cyclic softening behavior in the experimental steel.

Regarding to the fatigue crack propagation behavior, it is remarkable that the steel showed a poor fatigue crack growth resistance, i.e., high fatigue crack growth rate. The fatigue crack propagation behavior in the steel was actually examined by a pulsating stress ratio of 0.1 using compact tension (CT) specimens. The corresponding $da/dN - \Delta K$ obtained at 15 Hz in air is plotted in Fig. 10. Under the test condition, the crack growth evolution obeyed a Paris law, i.e., $da/dN = C\,\Delta K^m$. The corresponding C and m values were measured to be 26.7×10^{-32} and 22.8, respectively. Compared with other high-strength steels [24–26], whose m values are between 2.0 and 4.0, however, the present steel possessed a much higher m value of 22.8. It is well known that higher m value means poor fatigue crack growth resistance and higher fatigue crack growth rate. Therefore it can be assumed that maraging steels should behave in a similar fatigue crack propagation trend as TiAl intermetallics or ceramics, i.e., once a fatigue crack originated, a catastrophic failure will easily take place. This also implies that an increased yield stress obtained for highly alloyed ultra-high-strength steel does not always offer a substantial increase of the crack growth resistance. In other words, the fatigue crack growth resistance of steels with very high yield strength may be relatively poor. This phenomenon is of practical interest in view of selection of an ultra-high-strength material for structural application. It has already been pointed out by other researchers [18,25,26] that high-strength materials are often sensitive to fatigue notch, and now it appears that the fatigue crack growth resistance of the material may be critical. Therefore the designers should consider this aspect if they prefer to selecting a high-strength material for weight reduction or other reasons.

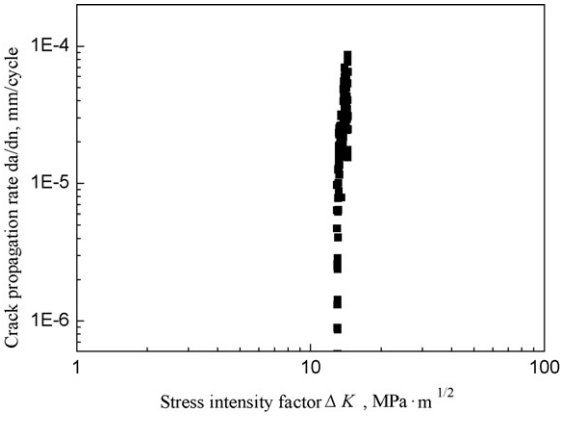

Fig. 10. Relationship between da/dN and ΔK.

In summary, the current experimental results can be explained that the cyclic softening of maraging steels is due to the resolution as well as the growth of precipitates in steels. The phenomenon of the multiplication and rearrangement of geometrically necessary dislocations, which can account for the monotonic hardening and the cyclic softening behaviors, was not found. More extensive TEM observation needs to be performed in order to reveal the mechanism of recovery from aging after the cyclic softening.

4. Conclusions

The main conclusions obtained from this study are summarized as follows:

1. A new 2.8 GPa grade maraging steel has been developed, which could reach an ultimate tensile strength of 2760 MPa and a fracture toughness of 31.6 MPa $m^{1/2}$.
2. The tension–tension fatigue property under peak-aging condition for the steel was experimentally examined by axial loading with stress ratio of 0.1, and a fatigue limit of 1150 MPa was obtained. Both the surface-induced fracture and the interior inclusion-induced fracture were found in the S–N characteristics of the steel.
3. The cyclic softening in the steel was confirmed by the enlarged size of the precipitates and the decreased ultimate tensile strength after cyclic deformation. The steel behaved in a poor fatigue crack growth resistance and high fatigue crack growth rate, i.e., the fatigue property of the steel was not as usually expected.

Acknowledgements

The authors would like to thank Prof. Z.G. Wang and Mr. G. Yao for their useful advices and experimental supports.

References

[1] K.V. Rajkumar, B.P.C. Rao, Mater. Sci. Eng. A 464 (2007) 233–240.
[2] V. Vijayk, S.J. Kim, C. Marvin Wayman, Metall. Trans. A 21 (1990) 2655–2668.
[3] F. Habiby, T.N. Siddiqui, H. Hussain, A. Ulhaq, A.Q. Khan, J. Mater. Sci. 31 (1996) 305–309.
[4] F. Habiby, T.N. Siddiqui, H. Hussain, A. Ulhaq, A.Q. Khan, Mater. Sci. Eng. A 159 (1992) 261–265.
[5] D.G. Lee, K.C. Jang, J.M. Kuk, I.S. Kim, J. Mater. Process. Technol. 162–163 (2005) 342–349.
[6] K. Hussain, A. Tauqie, A. ul Haq, A.Q. Khan, Int. J. Fatigue 21 (1999) 163–168.
[7] L.F. Van Swam, R.M. Pelloux, N.J. Grant, Metall. Trans. A 6 (1975) 45–53.
[8] Y. He, Yangke, W. Qu, F. Kong, G. Su, Mater. Lett. 56 (2002) 763–769.
[9] S. Floreen, G.R. Speich, Trans. ASM 57 (1964) 326–331.
[10] R. Tewari, S. Mazumder, I.S. Batra, et al., Acta Mater. 48 (2000) 1187–1200.
[11] M. Michihiko, T. Setsuo, J. Soc. Mater. Sci. Jpn. 497 (1995) 181–186.
[12] M. Hagiwara, Y. Kawabe, Trans. ISIJ 21 (1981) 422–428.
[13] Y. Kawabe, S. Muneki, K. Nakazawa, H. Yaji, Trans. ISIJ 19 (1979) 238.
[14] T. Yasuno, K. Kuribayashi, T. Haseqawa, J. ISIJ 84 (1998) 55–60.
[15] Y. Murakami, T. Nomoto, T. Ueda, Fatigue Fract. Eng. Mater. Struct. 22 (1999) 581–590.

[16] M. Nagumo, H. Uyama, M. Yoshizawa, Scr. Mater. 44 (2001) 947–952.
[17] Y. Murakami, T. Nomoto, T. Ueda, Fatigue Fract. Eng. Mater. Struct. 23 (2000) 893–910.
[18] M.D. Chapetti, T. Tagawa, T. Miyata, Mater. Sci. Eng. A 356 (2003) 227–235.
[19] K. Takai, Y. Homma, K. Izutsu, M. Nagumo, J. Jpn. Inst. Met. 60 (1996) 1155–1162.
[20] M. Michihiko, T. Setsuo, K. Noio, J. Soc. Mater. Sci. Jpn. 49 (2000) 631–637.
[21] M. Moriyama, T. Nagano, N. Kawagoishi, S. Takaki, J. Soc. Mater. Sci. Jpn. 50 (2001) 1126–1132.
[22] U.K. Viswanathan, R. Kishore, M.K. Asundi, Metall. Mater. Trans. A 27 (1996) 757–761.
[23] T.H. Courtney, Mechanical Behavior of Materials, 2nd ed., McGRAW-Hill Companies, Inc., 1990, pp. 574–583.
[24] D.Y. Wei, J.L. Gu, H.S. Fang, B.Z. Bai, Z.G. Yang, Int. J. Fatigue 26 (2004) 437–442.
[25] T. Sakai, Y. Sato, Y. Nagano, M. Takeda, N. Oguma, Int. J. Fatigue 28 (2006) 1547–1554.
[26] A Carpinteri, Int. J. Fatigue 15 (1993) 21–26.